Conformational Characterization of DnaK and Its Complexes by Small-Angle X-ray Scattering†

Li Shi,‡ Mikio Kataoka,§ and Anthony L. Fink*

Department of Chemistry and Biochemistry, The University of California, Santa Cruz, California 95064

Received August 21, 1995; Revised Manuscript Received December 1, 1995⊗

ABSTRACT: DnaK, a member of the 70 kDa heat shock protein (hsp70) family, and its complexes with substrate proteins and nucleotides were characterized by small-angle X-ray scattering (SAXS) and size-exclusion chromatography (SEC) techniques. The SAXS data indicated that DnaK has a dumbbell-shaped structure with a maximum dimension (d_{max}) of 112 Å, which is consistent with the reported two major functional domains [Chappell et al. (1987) *J. Biol. Chem. 268*, 12730−12735; Flaherty et al. (1990) *Nature 346*, 623−628]. The data were best fit by a model in which the two domains either are connected by a short hinge region or are just in contact with each other. The radius of gyration (R_g) of DnaK was determined as 37.5 ± 1.0 Å in the absence of nucleotide. Binding of ATP induces a conformational change in DnaK as reflected by the changes in its $P(r)$ function and Kratky plot, the increases (1−2 Å) in both its radius of gyration (R_g) and its Stokes radius (R_s), and the increase in its d_{max} (5−10 Å). SAXS and SEC−HPLC results indicate that the association state of DnaK is very sensitive to the buffer concentration and the presence of substrates, as well as the protein concentration. At high buffer and protein concentrations, DnaK dimerizes, resulting in an increase in its apparent R_g and d_{max} values. The addition of substrate (unfolded protein or ATP) results in a return to the R_g value of monomeric DnaK, due to the dissociation of DnaK multimers induced by the substrate binding and resultant conformational changes. The DnaK−substrate protein complex gives a smaller R_g than expected, suggesting that the substrate protein binds to a cavity or cleft on DnaK rather than the exterior of the chaperone. The Kratky plot of the Gdn·HCl-induced unfolding intermediate state of DnaK is consistent with a compact, molten globule-like conformation, as previously suggested based on CD, fluorescence, and SEC−HPLC results [Palleros et al. (1993) *Biochemistry 32*, 4314−4321].

Members of the hsp70 family of molecular chaperones have been recognized as critical factors in the routine functioning of cells, as well as in times of stress (Ang et al., 1991; Hartl et al., 1992; Gething & Sambrook, 1992; Welch, 1993; Morimoto et al., 1994). Constitutive functions include facilitating the folding, assembly, and membrane translocation of proteins in the cell (Kang et al., 1990; Hartl & Neupert, 1990; Getting & Sambrook, 1992; Hendrick & Hartl, 1993; Wickner, 1994; Ungermann et al., 1994; Ellis, 1994). Hsp70 proteins are present in prokaryotes and eukaryotes, and have been implicated in a wide variety of medically important phenomena, including viral infection, cancer and disorders of the immune system, and other conditions of cellular stress. The basic paradigm of their function is that they bind denatured or unfolded proteins (Bole et al., 1986; Getting et al., 1986; Liberek et al., 1991b), nascent polypeptide chains (Dorner et al., 1987; Beckmann et al., 1990), and short peptides (Flynn et al., 1989, 1991; Lam & Calderwood, 1992), which are then released upon the binding and hydrolysis of ATP.

As the major *Escherichia coli* member of the hsp70 family, DnaK was found to bind nucleotides and unfolded, but not folded, proteins (Bole et al., 1986; Gething et al., 1986; Liberek et al., 1991b; Palleros et al., 1992, 1994a; Shi, 1994). The association and dissociation of DnaK with substrate protein are regulated by ATP and ADP. This regulation was found to be dependent on the presence of both Mg^{2+} and K^+ (Palleros et al., 1993a) and accompanied by conformational changes (Palleros et al., 1994a). The presence of an unfolded substrate significantly increases the ATPase activity of hsp70 (Flynn et al., 1989; Sadis & Hightower, 1992; Blond-Elguindi et al., 1993; Palleros et al., 1993a), suggesting that substrate binding may affect the conformation of DnaK, leading to effects on the rate of ADP/ATP exchange.

Hsp70 proteins are highly conserved throughout evolution in both structural and functional properties (Gething & Sambrook, 1992; McKay, 1993; Hendrick & Hartl, 1993), and consist of two major functional domains (Chappell et al., 1987; Flaherty et al., 1990): a more conserved 44-kDa N-terminal domain which is responsible for nucleotide binding, and a more variable substrate protein binding C-terminal domain. Although the X-ray structure of the N-terminal domain of hsc70, the constitutive mammalian cytosolic member of the hsp70 family, has been solved (Flaherty et al., 1990; 1991), no structure of the complete molecule of any member of the hsp70 family has been reported. Several different shapes (including sphere, ellipsoid, triangle, square, and dumbbell) have been invoked

† This work was supported in part by a grant from the National Institutes of Health.

* To whom correspondence should be addressed.

‡ Present address: Department of Pharmaceutical Research, Merck Research Laboratories, WP78-302, West Point, PA 19486.

§ Present address: Department of Earth and Space Science, Faculty of Science, Osaka University, Toyonaka, Osaka 560, Japan.

⊗ Abstract published in *Advance ACS Abstracts,* March 1, 1996.

0006-2960/96/0435-3297$12.00/0

in the literature for hsp70 (Burdon, 1988; Liberek et al., 1990; Hartl & Neupert, 1990; LaRossa & Van Dyk 1991; Gething & Sambrook, 1992; Langer et al., 1992; Craig, 1993; Lane et al., 1993; Neupert & Pfanner, 1993; Dierks et al., 1993; Hendrick & Hartl, 1993; Frydman et al., 1994; Wickner, 1994; Palleros et al., 1994a), although no direct measurements have been reported. It has been proposed that the binding of ATP to hsp70 induces a conformational change which leads to the dissociation of bound substrate protein (Liberek et al., 1991a,b; Landry et al., 1992; Palleros et al., 1992, 1993a). The only spectroscopic evidence for establishing this conclusion was the observation of a blue shift in the DnaK tryptophan fluorescence spectrum induced by ATP. Further evidence is needed to support the proposed conformational changes induced by ATP, as well as substrate protein binding. Small-angle X-ray scattering (SAXS)[1] is the best available technique for characterizing the size, compactness, and shape of protein molecules in solution, and it is particularly valuable when the use of crystallography or NMR is precluded (Flanagan et al., 1992, 1993; Kataoka et al., 1993, 1994, 1995; Lattman, 1994), as in the present case. In addition to the overall radius of gyration (R_g) and the maximum dimension (d_{max}), SAXS can quantitatively describe the globular conformation of a protein molecule, as well as ligand-induced conformational changes in the protein. We report here the initial structural and conformational characterization of DnaK carried out by small-angle X-ray scattering.

EXPERIMENTAL PROCEDURES

Materials

E. coli DnaK was isolated and purified by a modification of procedures previously described (Cegielska & Georgopoulos, 1989; McCarty & Walker, 1991; Palleros et al., 1993b). The final purity of DnaK was greater than 98% as determined by SDS−PAGE, deemed adequate for the present study. The concentration of DnaK was determined by absorbance using an extinction coefficient of 27 000 (cm M)$^{-1}$ at 280 nm as previously described (Palleros et al., 1993b). RCMLA, reduced and carboxymethylated α-lactalbumin, was from Sigma. NCA-SNase, a mutant of staphylococcal nuclease containing a five amino acid type I β-turn from concanavalin A in place of residues 27−30 of SNase (Hynes et al., 1989), was a gift from Professor R. O. Fox. The concentrations of RCMLA and NCA-SNase were determined as previously reported (Palleros et al., 1991, 1992). ATP (disodium salt) was from Pharmacia LKB Biotechnology Inc. ADP (monosodium salt) was from Calbiochem. Nucleotide concentrations were determined by the absorbance at 259 nm using an extinction coefficient of 15 400 (cm M)$^{-1}$ (Fasman, 1983). ATP refers to an equimolar solution of $MgCl_2$ and ATP (disodium salt); ADP refers to an equimolar solution of $MgCl_2$ and ADP (monosodium salt), in Tris·HCl buffer containing a final concentration of 20 mM KCl. Guanidine hydrochloride (Gdn·HCl), ultrapure grade, was from ICN Biochemicals. Gdn·HCl concentrations were determined by the index of refraction as described elsewhere (Nozaki, 1972; Pace et al., 1989) using a Bausch & Lomb refractometer. All other chemicals were from the same sources as previously reported (Palleros et al., 1991, 1992).

Methods

Small-angle X-ray scattering measurements were performed as previously described (Kataoka et al., 1991, 1993, 1994, 1995) at 20 °C using the solution scattering station installed at BL10C at the Photon Factory, Tsukuba, Japan, with synchrotron radiation. The wavelength of the X-rays was adjusted to 1.488 Å, calibrated by the nickel absorption edge. The incident beam was focused by a bent cylindrical mirror to give a quasi-point focus. The sample scan time was 10−20 min. The protein concentration was varied from 0.6 to 7 mg/mL. Background traces were collected on identical solutions to the sample ones, with the exception that the protein was omitted. The sample cell was 80 μL in volume with 15 μm thick quartz windows, and a 1 mm path length.

The gyration radius (R_g) values were estimated by the Guinier approximation (Guinier, 1939), $I(Q) = I(0) \exp(-R_g^2Q^2/3)$, where Q and $I(0)$ are the momentum transfer vector and scattering intensity at zero scattering angle, respectively (Guinier & Fournet, 1955). Here Q is defined as $Q = (4\pi \sin \theta)/\lambda$ where 2θ and λ are the scattering angle and the wavelength of the X-rays, respectively.

The distance distribution function, $P(r)$, the frequency of vectors, r, connecting small-volume elements within the entire volume of the scattering particle, was calculated according to: $P(r) = {}^1/_2\pi^2 \int I(Q)Qr \sin(Qr)\, dQ$, using the indirect Fourier transform method of Moore (1980) and evaluated using the GNOM program of Svergun et al. (1988). In the calculation, the scattering intensity extrapolated to zero protein concentration was used as $I(Q)$ (Moore, 1980). From the $P(r)$ function, the maximum particle dimension, d_{max}, was estimated as the vector value, r, where $P(r)$ becomes zero. The R_g values were also estimated from the second moment of the $P(r)$ function according to the relationship $R_g^2 = \int P(r)r^2\, dr/2\int P(r)\, dr$.

SAXS sample preparation was as follows: DnaK stock solutions (in Tris·HCl, pH 7) were prepared in various buffer concentrations by exchange from 100 mM Tris·HCl using Centricon10 membranes. The protein solutions were stored at −70 °C and thawed on ice for SAXS measurements. Samples with nucleotide and salt (KCl) were incubated at room temperature for about 5 min before the measurements. Nucleotide concentrations were 1 mM with 20 mM KCl. Samples with substrate (RCMLA or NCA-SNase) were incubated at 37 °C for 30 min to form complex. All samples were centrifuged for a short time prior to analysis.

Size-exclusion HPLC experiments were carried out as previously reported (Palleros et al., 1992) using a Beckman instrument and a Bio-Sep 3000 silica column (600 × 7.8 mm, from Phenomenex). The HPLC mobile phase was 20 mM sodium phosphate, 200 mM KCl, pH 6.5, with a flow rate of 1 mL/min. Samples of 20 μL were injected into the HPLC and detected by the absorbance at 215 nm. Chromatograms were collected on a computer with an acquisition time of 1 point per second. For each species, the areas under

[1] Abbreviations: SAXS, small-angle X-ray scattering; CD, circular dichroism; R_g, radius of gyration; R_s, Stokes radius; d_{max}, maximum dimension of the protein molecule; SEC, size-exclusion chromatography; Gdn·HCl, guanidine hydrochloride; RCMLA, reduced, carboxymethylated α-lactalbumin; NCA-SNase, mutant of staphylococcal nuclease containing a five amino acid type I β-turn from concanavalin A in place of residues 27−30 of SNase (Hynes et al., 1989).

the curves were obtained by curve fitting of the chromatogram with the program LabCalc (Galactic Ind., Salem, NH), using Gaussian functions. Partition coefficients were calculated as $K_d = (V_i - V_o)/V_t$, where V_i is the protein elution volume, V_o is the void volume (elution volume of blue dextran), and V_t is the total solvent-accessible volume (elution volume of sodium azide).

Computer simulations of the distance distribution function [$P(r)$] were carried out using a protein structural model constructed of two spheres, either overlapping, in contact, or slightly separated (by a hinge or connecting region). The scattering intensities at small angles were calculated with the following formula: the scattering intensity from two spheres of radii R_1 and R_2 with a distance L between their centers is $I(s) = G(QR_1)G(QR_1) + G(QR_2)G(QR_2) + 2G(QR_1)G(QR_2)\sin(QL)/QL$, where $G(QR_1) = 4\pi R_1^3\{[\sin(QR_1) - QR_1\cos(QR_1)]/(QR_1)^3\}/3$, and $G(QR_2) = 4\pi R_2^3\{[\sin(QR_2) - QR_2\cos(QR_2)]/(QR_2)^3\}/3$.

Extrapolation to zero angle was accomplished by a computer program which takes the $I(Q)$ vs Q plots for a series of DnaK concentrations and extrapolates each $I(Q)$ point to zero protein concentration. These data are then used to extrapolate to zero angle.

RESULTS

Guinier Plots and Determination of R_g. The radius of gyration, R_g, of a protein molecule is usually calculated based on the slope of its Guinier plot, $\ln[I(Q)]$ versus Q^2, using the criterion of $Q^*R_g < 1$ or ≤ 1.3 (Guinier, 1939; Olah et al., 1993; Kataoka et al., 1995) or $Q < \pi/d_{max}$ (Marshall et al., 1994). However, Kataoka et al. (1995) have shown that the Guinier region of the scattering curve obtained for proteins usually extends to $Q^*R_g \leq 2$. Figure 1A shows the Guinier plots of DnaK in 1 mM Tris·HCl: the value of R_g, namely, 37.5 ± 1.0 Å, was the same when calculated from regions of the Guinier plots with $Q^*R_g < 1.2$ to < 1.8. To avoid possible effects of protein concentration on the determination of R_g, the scattering curves were measured at different DnaK concentrations, and the final values of R_g were determined by extrapolation to zero protein concentration, as shown in Figure 2. The data in Figure 2 also reveal that at buffer concentrations ≥20 mM Tris·HCl a small protein concentration dependence was observed. It is known that hsp70s, including DnaK, undergo self-association, especially at high protein concentration. In addition, as can be seen in Figure 2, increasing concentration of buffer led to increasing values of R_g. That this was due to an ionic strength effect was confirmed by size-exclusion HPLC, and glutaraldehyde cross-linking, which showed the absence of oligomers at low buffer concentration and increasing amounts of oligomers, especially the dimer, at higher salt concentrations, and in the presence of ADP (Shi, 1994). Table 1 shows the effect of different buffer concentrations on R_g. It can be seen from Figure 2 that the protein and buffer concentration effect became negligible when the buffer concentration was 1 mM.

When the Guinier plots were constructed for scattering data at higher angles, a change in the slope was observed (as shown in Figure 3). Our analysis of these plots as a function of buffer concentration indicates that two phenomena are occurring simultaneously: (1) at each buffer concentration, we observe a biphasic Guinier plot if both low- and high-angle data are included, reflecting the bilobed shape (see below) of DnaK; and (2) the slope of the small-angle region of the Guinier plot increases as the buffer concentration increases, reflecting the presence of some oligomers of DnaK.

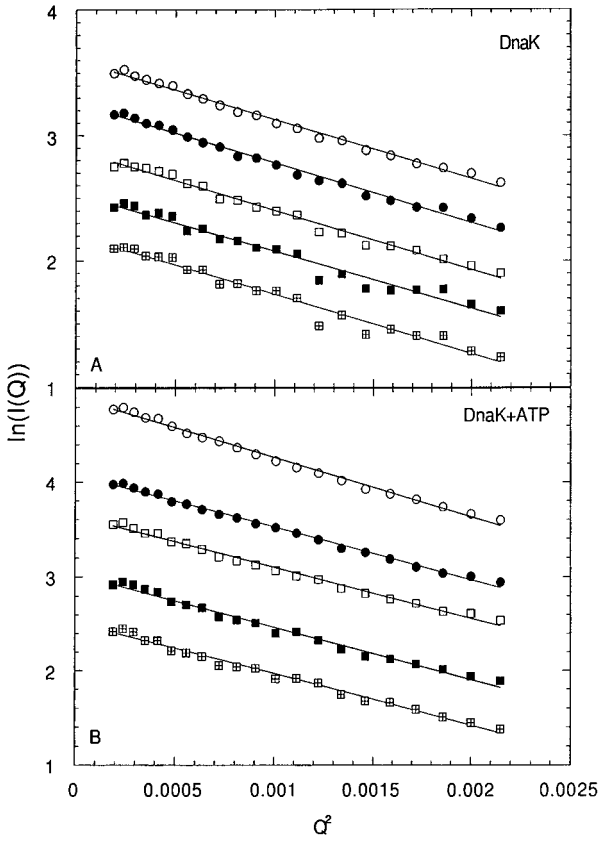

FIGURE 1: Guinier plots of X-ray scattering data for DnaK in 20 mM Tris·HCl (pH 7). Panel A, DnaK alone: panel B, DnaK with 1 mM Mg/ATP. The protein concentrations were (from top to bottom) 4.6, 3.0, 2.0, 1.0, and 0 mg/mL. The 0 mg/mL data were obtained by extrapolation from the higher concentrations. For clarity, the values of the individual plots have been shifted on the $\ln[I(Q)]$ axis. The region shown is for $Q^*R_g < 1.7$.

Both polydisperse systems and multidomain proteins may show Guinier plots with curvature (as seen in Figure 3) within an extended region overlapped with that normally used for R_g calculations. Quantitative analysis of a polydisperse system using a model of different size (R_g) homogeneous spheres (Feigin & Svergun, 1987) was applied to a polydisperse nitrogenase enzyme system (Eliezer et al., 1993a). It was shown that the effect of the larger aggregates in the system is negligible in the Guinier analysis at relative large angles which more closely corresponded to the real Guinier features of the monomer. Larger mass/size particles in solution absolutely dominate the scattering contribution at very small angles but have much less contribution to the scattering at relative high angles (Guinier & Fournet 1955).

R_g values for DnaK determined from both the small and large scattering angle phases of the Guinier plots, as a function of buffer concentration, are shown in Figure 4. The value of R_g increased with Tris·HCl concentration, leveling off at >100 mM (Figure 4, top curve). The R_g values calculated from the small-angle region of the Guinier plot indicate that there is no major population of scattering particles with a size larger than the dimer of DnaK. Also, experiments carried out at very small angles indicated that

Table 1: R_g Values for DnaK and Its Complexes Determined by Guinier Approximation and $P(r)$ Function

	[Tris·HCl]							
	1 mM			20 mM			50 mM	100 mM
	R_g (Å), Guinier	R_g (Å), $P(r)$	d_{max} (Å)	R_g (Å), Guinier	R_g (Å), $P(r)$	d_{max} (Å)	R_g (Å), Guinier	R_g (Å), Guinier
DnaK	37.5 ± 1.0	37.9 ± 1.0	112 ± 5	46.2 ± 1.0	47.0 ± 1.5	150 ± 5	51.1 ± 1.0	55.3 ± 1.5
+ATP	39.8 ± 1.0	40.5 ± 1.0	123 ± 5	40.7 ± 1.0				
+ADP	45.4 ± 1.5							
+RCMLA	42.3 ± 1.0	41.6 ± 1.5	132 ± 5	43.7 ± 1.0	43.7 ± 1.0	132 ± 5		
+SNase	42.1 ± 1.0	42.9 ± 1.5	125 ± 5	42.0 ± 1.0	42.6 ± 1.0	125 ± 5		
Gdn·HCl	(0.8 M)			53.0 ± 1.5				
Gdn·HCl	(4.0 M)			69.0 ± 2.0				

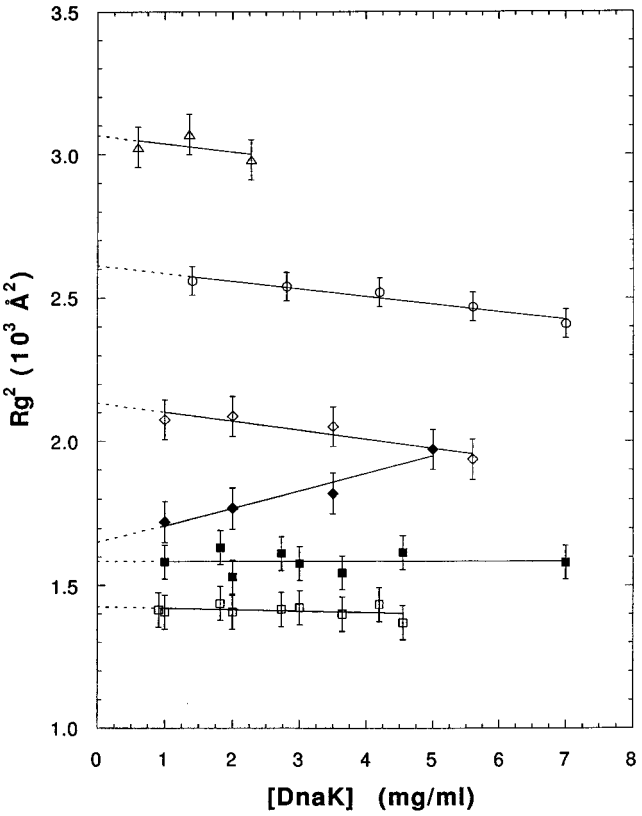

FIGURE 2: Radii of gyration as a function of DnaK protein concentration in various concentrations of Tris·HCl buffer, and in the presence (filled) and absence (open) of ATP. The concentrations of Tris·HCl are (from top to bottom) 100 mM (triangles), 50 mM (circles), 20 mM (diamonds), and 1 mM (squares). The final R_g values were determined based on the intercepts (at zero protein concentration) of the linear fitting. The nucleotide concentration was 1 mM.

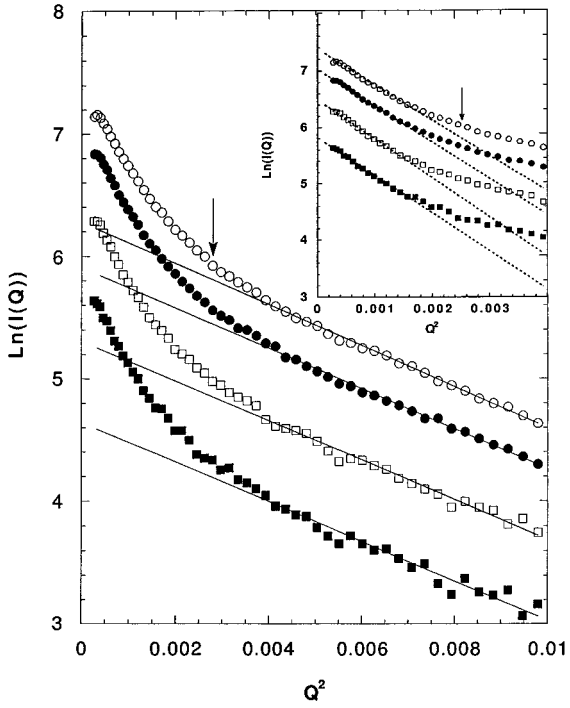

FIGURE 3: Guinier plots of X-ray scattering data for DnaK in 20 mM Tris·HCl (pH 7). Protein concentrations are (from top to bottom) 5.6, 3.05, 1.7, and 0.9 mg/mL. The solid lines measure the slopes of Guinier plots at the larger scattering angles, and the dashed lines (inset) measure the slope of the Guinier plots at the smaller scattering angles (note different Q^2 scales). The arrow roughly shows the turning point between the larger and smaller scattering angle phases of the curves. The region shown is for $Q^*R_g < 1.88$.

there is no aggregated form of DnaK present in 1 mM Tris·HCl solution. The general features of the Guinier plots of DnaK as a function of buffer concentration were the same for 20 mM Tris and higher. The plots of $C/I(0)$ versus protein concentration, C, for all DnaK samples (see Figure 11) were acceptably linear, suggesting that there are no significant changes in protein mass or size distribution in the experimental protein concentration range.

The analysis of the Guinier plots is complicated because there are two phenomena occurring: self-association at higher buffer concentrations, and a dumbbell-shaped molecule. Our interpretation is that the underlying biphasicity reflects a dumbbell-shaped structure, and the increasing slope at small values of Q^2 reflects the presence of dimer. For example, at 1 mM Tris buffer, where the Guinier plots at low angles are quite linear, reflecting the lack of any association of DnaK, the biphasicity observed when larger angle scattering is included in the Guinier plots is similar to that shown by dumbbell-shaped molecules such as calmodulin (Heidorn & Trewhella, 1988; Kataoka et al., 1991), and reflects the multidomain structure of DnaK. In the Guinier plots, at 1 mM Tris·HCl buffer concentration, the data at the smallest angles ($Q^2 < 0.002$) reflect the contribution of monomeric DnaK ($R_g = 37-38$ Å), and the data at higher angles reflect the individual domains of the DnaK molecule ($R_g = 22-24$ Å). At high Tris·HCl concentrations, the data at lowest angle show indications of slight upward curvature due to the presence of associated DnaK (dimer) ($R_g = 46-55$ Å). Figure 4 shows the R_g values calculated from the lower and higher angles of the Guinier plots as a function of Tris·HCl concentration. Only the first phase is affected by the buffer concentration. Table 1 shows the R_g values determined by both Guinier plot and $P(r)$ function under various conditions. As expected for a monodisperse solution, at low Tris·HCl (1 mM) concentration, there is a good agreement between the R_g values obtained by the Guinier approximation and the $P(r)$ function analysis.

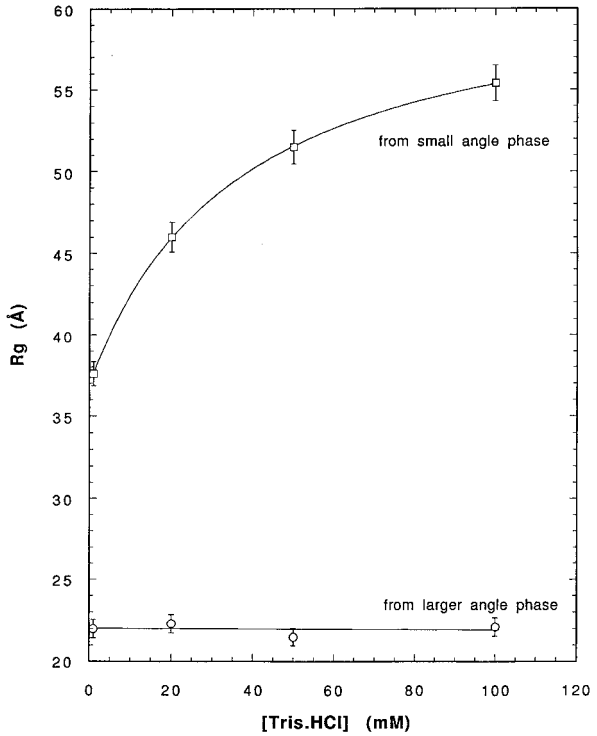

FIGURE 4: Radii of gyration as a function of buffer (Tris·HCl) concentration. The data points of the top curve (squares) were derived from the small scattering angle phase of the Guinier plots (e.g., Figure 1 inset, dashed line); the data points of the bottom curve (circles) were derived from the larger scattering angle phase (e.g., Figure 1, solid line).

SEC−HPLC Measurements of R_s: Effects of Nucleotides and Substrate Protein. Figure 5 shows the effects of ATP and substrate proteins on the elution volumes of DnaK in SEC−HPLC. It can be seen that the formation of a complex between DnaK and substrate protein results in the disappearance of the DnaK dimer peak. The disappearance of the dimer peak was also observed when ATP was added to DnaK. In addition, a small decrease in DnaK elution volume, corresponding to a 1−2 Å change in R_s, was observed with ATP bound (both ATP and ADP bind to DnaK with submicromolar dissociation constants). On the other hand, the addition of ADP enhances the self-association of DnaK, but has no effect on the elution volume of monomeric DnaK (data not shown). The effects of nucleotides and protein concentration on the oligomeric state of DnaK were confirmed by native PAGE and glutaraldehyde cross-linking experiments. SEC−HPLC analysis of the effect of buffer concentration on the association state of DnaK indicates that at high Tris·HCl concentration (100 mM) 20−50% of the DnaK is present as dimer or trimer, depending on the protein concentration. However at low Tris·HCl concentration (1 mM), more than 95% DnaK is in its monomeric form, even when the protein concentration is as high as 200 μM (Shi, 1994).

Based on the HPLC elution volume of each species, the hydrodynamic radii, R_s (Stokes radius), of the DnaK monomer and dimer and the DnaK−RCMLA and DnaK−NCA-SNase complexes were calculated (Palleros et al., 1994b) as 41 Å, 56 Å (see footnote 2).[2] 52 Å, and 51 Å, respectively.

Radial Distribution P(r) Function and Determination of d_{max}. Perhaps the most useful analysis of the shape of protein molecules with small-angle X-ray scattering data is the radial or distance distribution function, $P(r)$. Figure 6 shows the

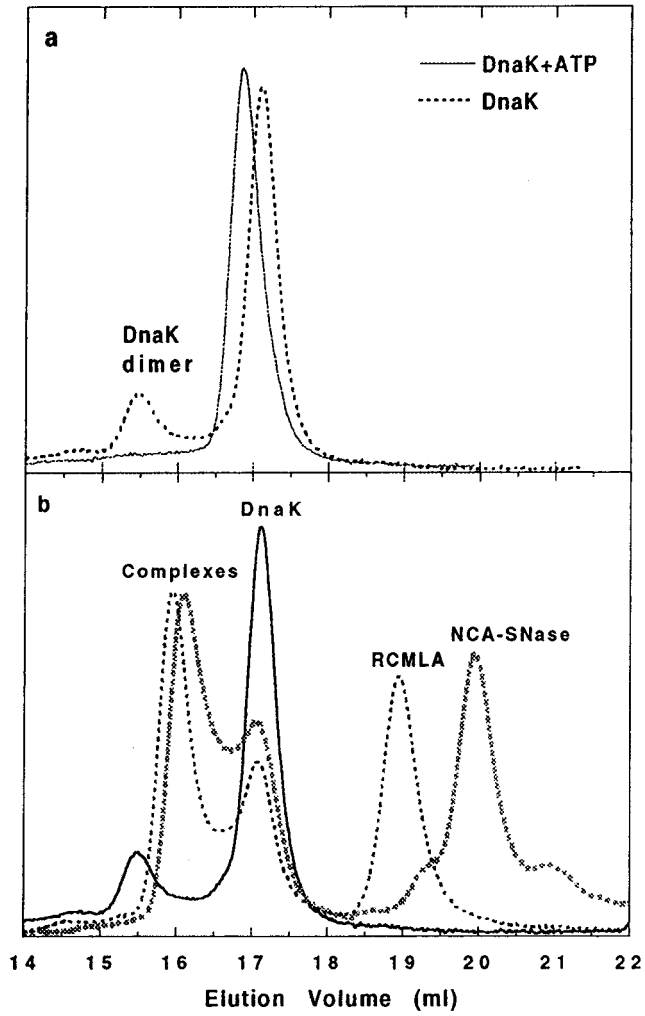

FIGURE 5: SEC−HPLC traces of DnaK and its complexes with substrates. (a) DnaK in the presence (solid line) and absence (dashed line) of ATP. (b) DnaK (solid line), DnaK + RCMLA (light broken line), and DnaK−NCA-SNase (dark broken line). All samples were in 100 mM Tris·HCl buffer (pH 7) with the following final concentrations: DnaK, 20 μM; NCA-SNase and RCMLA, 25 μM; ATP, 1 mM. DnaK−substrate protein complexes were formed by incubating at 37 °C for 30 min before HPLC injections. The mobile phase was 200 mM KCl, 25 mM Na_2HPO_4, pH 6.5. The sample injection volume was 20 μL. Eluant was monitored at 215 nm. The dilution factor of HPLC was estimated as 50.

$P(r)$ functions of DnaK in 1 mM (solid circles) and 20 mM (open circles) Tris·HCl buffers, respectively. At low Tris·HCl concentration, the $P(r)$ function is bimodal, with a d_{max} of 112 Å. However, when the Tris·HCl concentration is increased to 20 mM ,the $P(r)$ function becomes trimodal, and d_{max} is increased to 150 Å. For both cases, the R_g values are in good agreement with those obtained by Guinier approximation (Table 1).

Effects of Substrate Binding. Figure 1B shows the Guinier plots for DnaK in the presence of ATP. Calculation of R_g yields a marginally larger value of 39.8 ± 1.0 Å, compared to the free chaperone (Table 1). Figure 7 shows the $P(r)$ functions of DnaK in the presence (open circles) and absence (filled circles) of ATP. It can be seen that the presence of 1 mM ATP (K^+, Mg^{2+}) results in a shift in the $P(r)$ curve,

[2] The apparently small value for the dimer relative to the monomer can be explained in the context of the dumbbell-shaped molecule: a possible analogy would be the packing of two snowmen (small domain = head, large domain = body) with one upside down, i.e., ⇅.

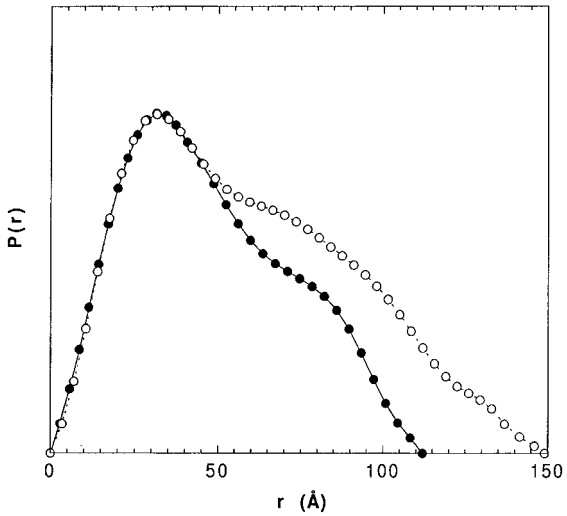

FIGURE 6: Distance distribution function, $P(r)$, plots of DnaK in low (1 mM, filled circles) and high (20 mM, open circles) Tris·HCl solution. The $P(r)$ function intensity is in arbitrary units.

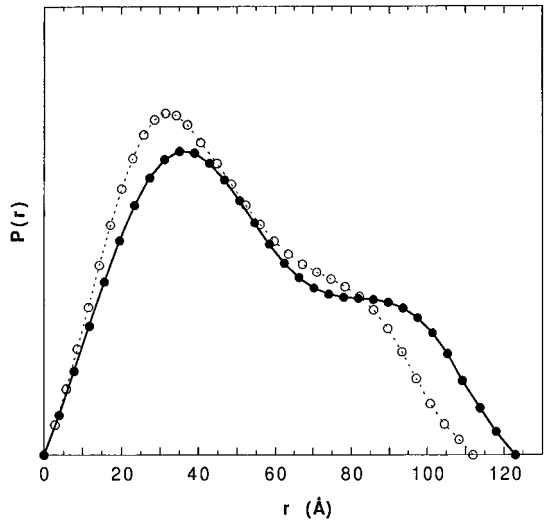

FIGURE 7: Distance distribution function, $P(r)$, plots of DnaK in the presence (filled circles) and absence (open circles) of ATP (1 mM) in 1 mM Tris·HCl (pH 7) buffer. The intensity of the $P(r)$ function was normalized to the same total area.

corresponding to a 5−10 Å increase in d_{max}. The radial distribution plots of the DnaK−RCMLA and DnaK−NCA-SNase complexes are shown in Figure 8. The binding of RCMLA results in no significant shift in the major peak of DnaK, but an increase in d_{max} by 20 Å. On the other hand, the binding of NCA−SNase results in a shift of the major peak of DnaK to larger distance and an increase in d_{max} by 15 Å. This results in an overall $P(r)$ function shape change which is not clearly seen for the DnaK−RCMLA complex. Note that under the conditions of the SAXS data collection (20 °C) the RCMLA is still unfolded, whereas the SNase would be in its native conformation if it were not bound to DnaK: recent CD and fluorescence experiments indicate that the bound SNase, at 20 °C, is in a substantially unfolded conformation (Palleros et al., 1994a).

DnaK Structure Models To Fit P(r). The interpretation of small-angle scattering data is mainly based on the comparison of experimental data with those of the model functions, e.g., Beltran et al. (1990). Various models of DnaK were investigated, in which the two domains were represented by unequal spheres. Only those model structures

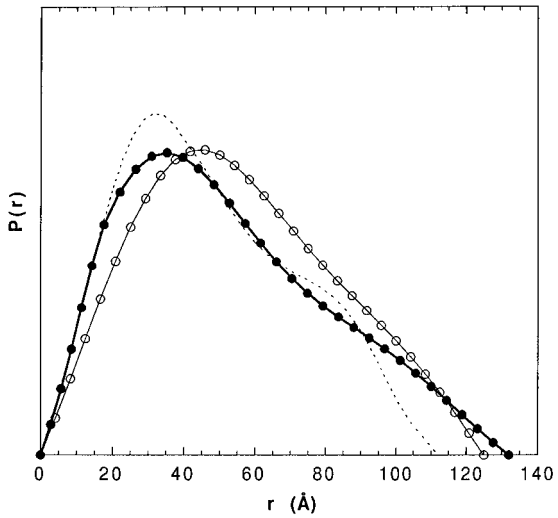

FIGURE 8: Distance distribution function, $P(r)$, plots of DnaK (dashed line), DnaK−RCMLA complex (filled circles), and DnaK−NCA-SNase complex (open circles) in 1 mM Tris·HCl (pH 7). The complexes were formed by incubation at 37 °C for 30 min. The intensity of the $P(r)$ function was normalized to the same total area.

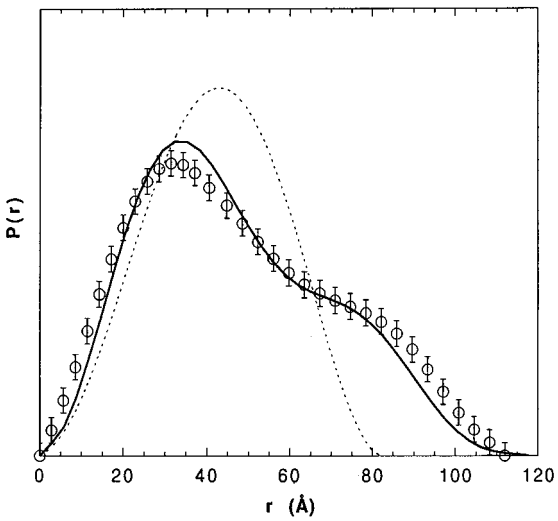

FIGURE 9: Comparison of the experimentally determined $P(r)$ function for DnaK with those calculated for two-sphere models (see text). Open circles, experimental data; solid line, calculated for a model of two unequal spheres (R_1 = 26 Å, R_2 = 32 Å) in close contact (L = 58 Å); dashed line, calculated for a model with one sphere (R = 41 Å, the R_s of DnaK).

in which the two spheres were in contact, or slightly separated (as by a short hinge region), fit the $P(r)$ data. In these models R_1 and R_2 represent the radii of the large and small domains, respectively, and L is the distance between the centers of the spheres (see Experimental Procedures). The scattering intensity was calculated as a function of Q, and then the theoretical $P(r)$ function was obtained using the GNOM program (Svergun et al., 1988). The calculated $P(r)$ function matched the experimental $P(r)$ function of DnaK best when R_1, R_2, and L have values in the range 32−34, 26−28, and 58−60 Å, respectively. Using R_1 = 32 Å, R_2 = 26 Å, and L = 58 Å, a value of 36.9 Å was obtained for R_g (Figure 9). This model is obviously an oversimplification, in that the two domains will not be true spheres. In fact, using the X-ray structure for the ATP domain of hsc70 (Flaherty et al., 1990) and a model of the C-terminal domain of DnaK based on the MHC peptide binding domain, we calculate R_g and d_{max} values of 21 and 70 Å for the ATP

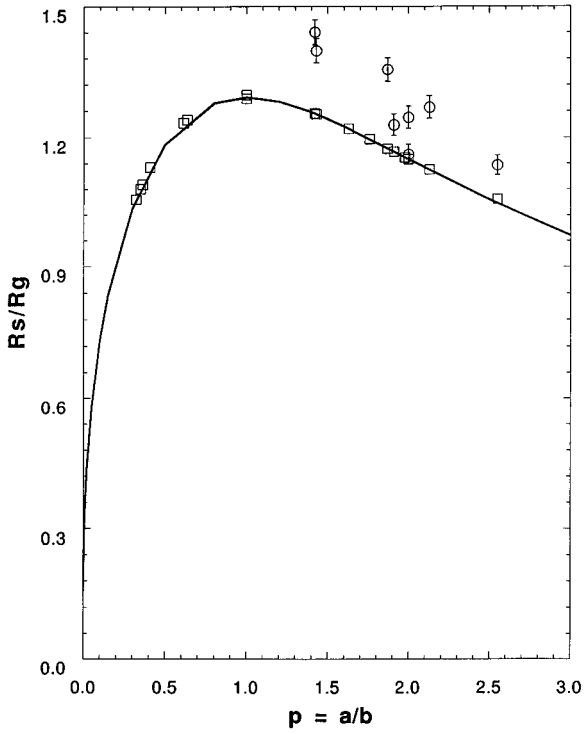

FIGURE 10: Relationship between R_s/R_g ratio and protein shape factor, $P = a/b$ (see text). The data points are experimental data based on sedimentation (circles) and SAXS (squares) measurements (Kumosinshi & Pessen, 1985). The solid line is the theoretical result calculated based on the equation: $R_s/R_g = P^{1/3}[5/(P^2 + 2)]^{1/2}$.

domain and 16.8 and 57.5 Å for the C-terminal domain, respectively. The R_g for the intact molecule can be estimated by the expression $R_g^2 = R_g(\text{ATP domain})^2 + R_g(\text{C-terminal domain})^2 + L^2/4$, from which $R_g = 41.7$ Å is obtained. For comparative purposes, Figure 9 also shows the expected $P(r)$ plot for a model in which DnaK is assumed to be spherical, with a radius equal to the measured Stokes radius of 41 Å.

Relationship between R_s, R_g, and the Shape of the Molecule. The relationship between R_s and R_g is quite sensitive to the shape and compactness of the protein. Based on the definition of the scattering volume of a hydrated macromolecule, $V = {}^4/_3\pi R_s^3$, and the relationship between the shape (sphere, oblate, or prolate ellipsoid), the radius of gyration (R_g), and the scattering volume of a protein (Kumosinshi & Pessen, 1985; Luzzati et al., 1961), the relationship between R_s and R_g is given by $R_s/R_g = P^{1/3}[5/(P^2+2)]^{1/2}$, where $P = a/b$, and a and b are the semiaxis of the revolution of the ellipsoid and the equatorial radius of the ellipsoid, respectively. For an ideal spherical structure, $a = b$, then $P = 1$, and the above equation gives $R_s/R_g = 1.29$ (Gast et al., 1994). A value of 1.25 was given by Gast et al. (1994) for "average" globular proteins. Figure 10 shows a plot of R_s/R_g vs P; the data points are based on experimentally measured protein diffusion coefficients, $D_{20,w}$ (sedimentation method), in water (to determine $R_s = kT/6D_{20,w}$) and SAXS (to determine R_g). Using this relationship, we find that since DnaK has an R_s/R_g ratio of 1.08, its overall a/b ratio is around 2.3 (assuming a prolate ellipsoid). This value is very consistent with the values of the domain radii from the best models to fit the $P(r)$ data.

Determination of the Relative Protein Scattering Particle Mass. The mass and the mass change of scattering particles can be determined by the scattering intensity at zero

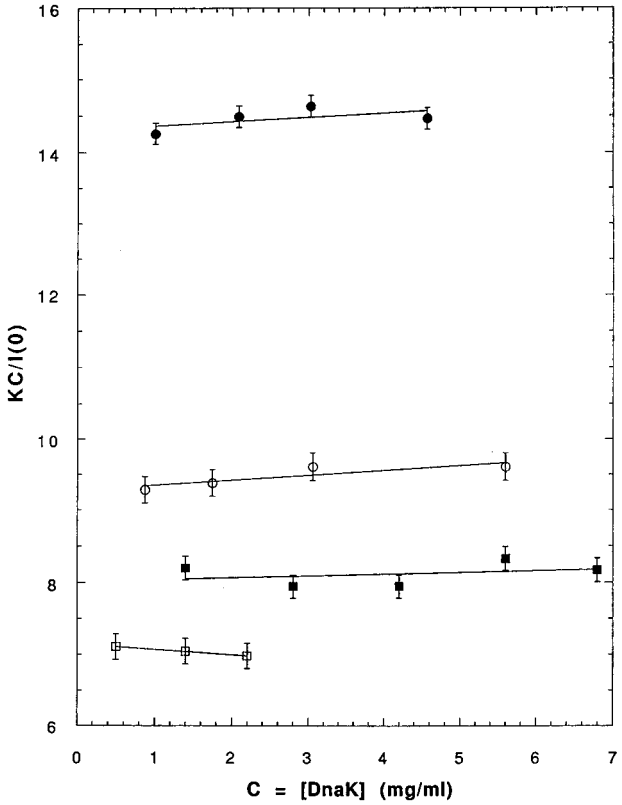

FIGURE 11: Scattering intensity at zero angle as a function of protein concentration: The relative mass of the protein as a function of buffer (Tris·HCl) concentration. Tris·HCl concentrations (from top to bottom) are 1, 20, 50, and 100 mM, respectively. K is a constant for all plots. The relationship between $C/I(0)$ and C is given in the text.

scattering angle with the relationship: $KC/I(0) = 1/M + 2A_0C$, where C is protein concentration in milligrams per milliliter; M is the apparent molecular mass of the scattering particle, A_0 is the second viral coefficient, and K is a constant. At zero protein concentration ($C = 0$), the intercept of a $KC/I(0)$ vs C plot gives $1/M$. From a reference protein of known molecular weight, M_r, the molecular weight of the sample protein, M_s, can be obtained from $[C/I(0)_r]/[C/I(0)_s] = M_s/M_r$ at $C = 0$. Figure 11 shows plots of $KC/I(0)$ vs C for DnaK in 1, 20, 50, and 100 mM Tris·HCl, respectively, revealing the apparent mass change in DnaK with increasing Tris·HCl concentration. The change in mass from lowest concentration (1 mM Tris) to highest (100 mM Tris) indicates a doubling in mass, consistent with a monomer and dimer at these extremes.

Kratky Plot for DnaK. The Kratky plot is a useful tool in the analyzing protein conformational change based on small-angle X-ray scattering data (Kataoka et al., 1993; Lattman, 1994). Figure 12 shows Kratky plots of DnaK at different Tris·HCl concentrations, and in the presence and absence of ATP. The addition of ATP (K^+, Mg^{2+}) results in a shift of the whole plot to smaller Q. Kratky plots are very useful because they reveal the nature of the protein conformation density (Kataoka et al., 1993). Figure 13 shows the Kratky plots of DnaK in 0.0, 0.6, and 1.5 M Gdn·HCl. The small-angle X-ray scattering of DnaK in >4 M Gdn·HCl was also measured, but its Kratky plot could not be analyzed in the larger angle region due to the poor S/N caused by the strong X-ray absorbance at high concentration of Gdn·HCl (although the small-angle region data were suitable for estimation of R_g with the Guinier approximation) (Table 1).

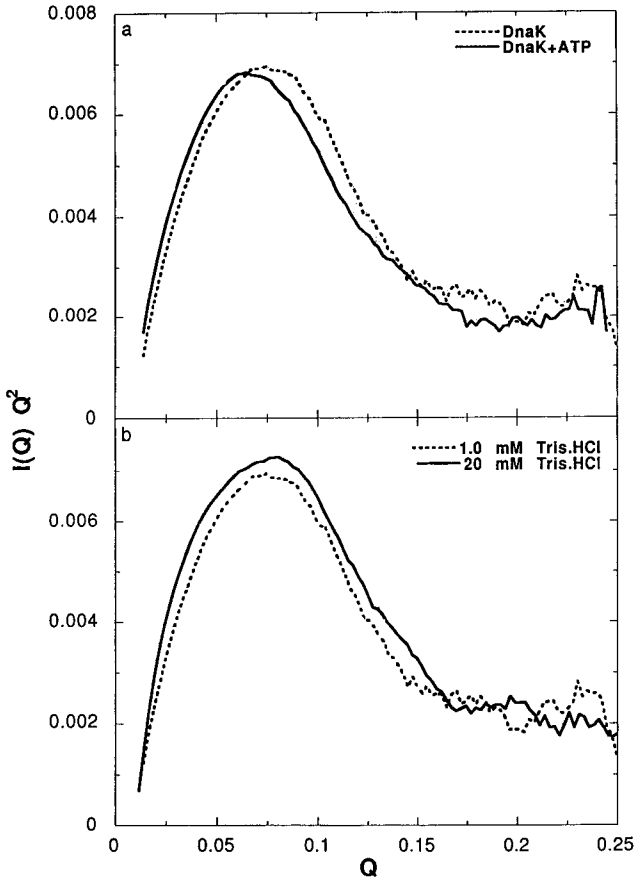

FIGURE 12: Kratky plots of scattering curves from DnaK (a) in the presence (dashed line) and absence (solid line) of ATP in 1 mM Tris·HCl solution, (b) in 1 mM (dashed line) and 20 mM (solid line) Tris·HCl solution (no ATP). The protein and nucleotide concentrations are described under Experimental Procedures.

The shape of the Kratky plot for DnaK shown in Figure 12 is characteristic of dumbbell-shaped proteins (Kataoka et al., 1995). Usually the innermost shoulder reflects the compact nature of the whole molecule, and the peak reflects the contribution of each domain. A Kratky plot with two distinct maxima is seen more clearly in the calculated intensity for the models with two distinct hydrophobic cores [see Figure 5 in Lattman et al. (1994)]. For a spherical single-domain protein, the Kratky plot shows a single peak with no shoulder. A very clear description on the relationship between the bimodal character of the Kratky plot and protein shape has been given recently by Kataoka et al. (1995). The Kratky plots in Figure 12 indicate that DnaK is dumbbell-shaped, and that binding of ATP affects the conformation; in addition, they indicate that native DnaK has the typical compact core of a globular protein, that DnaK denatured in 1.5 M Gdn·HCl is significantly unfolded, but retains some structure, as manifested by the shoulder in the vicinity of $Q = 0.075$, and that the partially-folded intermediate in 0.6 M Gdn·HCl has properties of both a folded protein and a molten globule-like state.

DISCUSSION

DnaK Is a Dumbbell-Shaped Molecule. DnaK is known to consist of two functional domains: the N-terminal ATPase domain and the C-terminal substrate binding domain, which are readily separated by proteolytic cleavage. The distance distribution function $P(r)$ of DnaK shown in Figure 6

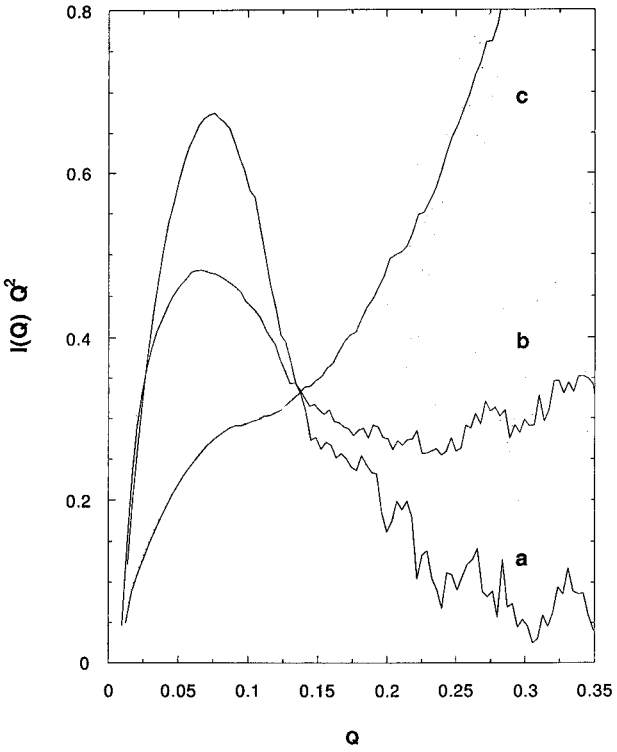

FIGURE 13: Kratky plots of scattering curves from various conformational states of DnaK (a) native DnaK in 1 mM Tris·HCl, pH 7; (b) partially-folded intermediate of DnaK in 0.6 M Gdn·HCl; (c) unfolded DnaK in 1.5 M Gdn·HCl. The solid lines are the results of smooth fitting of the experimental data.

indicates that DnaK is a dumbbell-shaped protein. A bimodal $P(r)$ distribution function plot is usually direct evidence of a dumbbell structure. The first peak represents the interatomic distance within each domain; the latter shoulder or peak represents the interdomain atomic distance (Kataoka et al., 1991). Both the Guinier plot and $P(r)$ function of DnaK give a radius of gyration (R_g) of 37−38 Å, which is larger than that of BSA (30 Å), although these two proteins have similar molecular weight. Since BSA is known to be somewhat elongated, the even larger R_g for DnaK indicates that the shape of the molecular chaperone must deviate significantly from a typical relatively spherical globular protein. The nonspherical nature of DnaK is also clear from the small value of R_s/R_g. For a spherical protein molecule, R_s/R_g is 1.29; the R_s/R_g for DnaK, 1.08, corresponds to an a/b ratio of 2.3, indicative of a prolate ellipsoid structure, which is consistent with a structure consisting of two spheres in close contact. From the $P(r)$ plot, it can been seen that the maximum dimension of DnaK is about 110 Å, consistent with an elongated shape with an average equatorial radius of 25−30 Å.

The dumbbell structure of DnaK is further evidenced by the following distinct features: (1) DnaK gives a biphasic Guinier plot (Figure 3) (Fujisawa et al., 1987; Kataoka et al., 1989, 1991), for which the smaller angle region gives the R_g value of the whole DnaK protein (37−38 Å for the monomer in 1 mM Tris·HCl), whereas the higher angle region gives the R_g value (22−24 Å) usually correlated to the size of individual domains of the dumbbell. Calmodulin is a typical dumbbell-shaped protein as shown by its $P(r)$ function (Kataoka et al., 1991; Heidorn & Trewhella, 1988), NMR (Ikura et al., 1990), and X-ray crystal structural data (Babu et al., 1985). Its Guinier plot shows a significant

biphasic curve. However, once it forms a complex with substrate, its $P(r)$ function shows a globular structure and its Guinier plot becomes monophasic (Kataoka et al., 1991, 1989), consistent with its crystallographic structure. (2) The Kratky plot of DnaK is also consistent with a bimodal shape, as can be seen from Figure 12. A similar shaped Kratky plot was observed for partially unfolded apomyoglobin which contains a compact helical core joined to a relatively random coil tail (Jennings & Wright, 1994; Kataoka et al., 1995). Calculations for a two-core structure model give a bimodal $P(r)$ function, and a bimodal Kratky plot with the shoulder peak at the innermost position (Lattman et al., 1994), as noted for DnaK. Similar modeling with a one-core model gives a unimodal $P(r)$ plot and a Kratky plot with a single maximum. For example, the bimodal character of DnaK becomes more significant at high Tris·HCl concentrations where DnaK tends to form a dimer, as discussed below. (3) The $P(r)$ function calculated using a model of two spheres in close contact gives an excellent match with the experimentally measured $P(r)$ function of DnaK, as shown in Figure 9. Also, as expected, the $P(r)$ function calculated using a one-sphere model does not agree with the experimental $P(r)$ function. (5) Preliminary electron microscope measurements show DnaK to be a molecule with an elongated ellipsoid-like shape with an a/b ratio of about 2 and a size of about 45 ± 5 Å $\times$ 110 ± 10Å (data not shown). An alternative explanation for the bimodal $P(r)$ function is that DnaK is in the form of a dimer. This possibility can be easily eliminated since the R_g obtained from the $P(r)$ function is a reasonable value for a monomeric DnaK molecule (as compared with that of BSA monomer) but not a dimer.

Size of the DnaK Molecule. As can be seen from Figure 4 and Table 1, the R_g of native DnaK monomer (in 1 mM Tris·HCl) is found to be 37.5 ± 1.0 Å. R_g values measured by SAXS are usually in agreement within 1−3 Å with those calculated from the X-ray crystal structure (Kataoka et al., 1995). Although the X-ray structure of the N-terminal domain of hsp73, a mammalian homologue of DnaK, has been solved, the structure for an intact hsp70 is not yet available. Therefore, calculation of the DnaK scattering function and its R_g is impossible at this time. However, BSA provides a good reference for analysis of the DnaK R_g value, since BSA has a similar molecular mass (67 kDa) to DnaK (69 kDa). The Stokes radius, R_s, of BSA is 34 Å (Palleros et al., 1993b; Corbett & Roche, 1984), and its R_g is 30 Å (Kumosinski & Pessen, 1985). DnaK has a Stokes radius of 41 Å, significantly larger than that of BSA, corroborating the larger R_g for DnaK. The difference between the R_g values of DnaK and BSA is mainly due to the dumbbell-shaped structure of DnaK in comparison to the more globular structure of BSA.

Effect of Buffer Concentration on the R_g Value of DnaK. The effects of protein aggregation and association are potentially significant and not uncommon problems in protein SAXS data analysis and interpretation (Chen et al., 1994; Eliezer et al., 1993). Most hsp70 proteins have been shown to exist as monomers, dimers, and trimers in a concentration-dependent equilibrium, a process which is strongly dependent on the presence of nucleotides. ATP, but not ADP, dissociates oligomers to monomers (Schmid et al., 1985; Hendershot et al., 1988; Palleros et al., 1991, 1992; Blond-Elguindi et al., 1993; Kim et al., 1992). Our results indicate that the association state of DnaK is also very sensitive to the nature of the buffer. This sensitivity is not due to the presence of nonspecific aggregation, but rather to the formation of DnaK dimers. The R_g of 37.5 Å was obtained under conditions where the size distribution of the protein is monodisperse; it is under such conditions that the $P(r)$ function gives the maximum length of DnaK as 112 Å.

For obtaining absolute structure parameters of a protein sample, the solutions must be monodisperse. In the case of DnaK at high Tris·HCl concentration (>20 mM), the R_g values obtained from analysis of the Guinier plot represent an average R_g (Glatter & Kratky, 1982) due to the polydispersity of the DnaK solution. Under these conditions, the particle mass value is a weight average, and the R_g value is a Z-average (Glatter & Kratky, 1982). For a monodisperse solution, the dimension of the protein can be determined to an accuracy of 1 Å (Glatter & Kratky, 1982; Muller et al., 1972), and conformational changes induced by substrate binding resulting in differences of a 1 Å change in R_g have been observed in hexokinase and phosphoglycerate kinase (McDonald et al., 1979; Pickover et al., 1979).

According to the relationship $KC/I(0) = 1/M + 2A_0C$ (Figure 9), at zero protein concentration, $KC/I(0) = 1/M$. Since $[C/I(0)_r]/[C/I(0)_s] = M_s/M_r$, we assign the $C/I(0)$ of DnaK in 1 mM Tris·HCl as $C/I(0)_r$ and those at higher Tris·HCl concentration as $C/I(0)_s$. Then the ratios of DnaK sample mass to DnaK molecular weight, M_s/M_r, are 1, 1.5, 1.8, and 2 for DnaK in 1, 20, 50, and 100 mM Tris·HCl buffer, respectively. The application of the above equation is based on the assumption that both high- and low-mass protein particles have the same electron density and hence partial specific volume. Thus, the mass of the DnaK protein scattering particles was doubled when the Tris·HCl concentration increased from 1 to 100 mM, and the mass increase parallels the increase in R_g with Tris·HCl concentration (Figure 4). The good linear correlation of the data points in the $KC/I(0)$ versus C plot (Figure 11) indicates that there is no significant nonspecific aggregation in the system, and that the solution is composed of monomer and dimer in equilibrium (possibly with some trimer at the higher concentrations). The uncertainty in sample mass determinations is in the range of 5−10% (Kaumaya et al., 1990).

Since SAXS is sensitive to changes in the size, shape, and density of the scattering molecules, the difference in I(0) must be caused by some of the above factors. Theoretically, protein conformational change does not affect $I(0)$, although it does affect the whole SAXS profile. No difference in CD and fluorescence spectra of DnaK is observed as a function of Tris·HCl concentration. Therefore, the change in $KC/I(0)$ toward zero protein concentration is not due to the conformational change of the scattering particle, but reflects the dissociation/association of DnaK. This is further confirmed by SEC−HPLC analysis, which shows that at 1 mM Tris·HCl DnaK is in its monomeric state, and at high Tris·HCl concentration DnaK associates into oligomers (dimer mainly, and some trimer).

ATP Induces a Conformational Change in DnaK. At high Tris·HCl concentration, the addition of ATP results in a significant decrease in the observed R_g for DnaK (Figure 2 and Table 1). However, at low Tris·HCl concentration, the addition of ATP results in an increase in R_g. These opposite results are readily explained as follows, based on our understanding of the system (Palleros et al., 1994):

At high Tris·HCl concentration, DnaK associates to form oligomers; the addition of ATP causes their dissociation (Figure 5a), resulting in a decrease in the measured R_g. This dissociation effect of ATP on DnaK multimers has been observed previously (Schmid et al., 1985; Hendershot et al., 1988; Kim et al., 1992; Palleros et al., 1993c; Blond-Elguindi et al., 1993). At low Tris·HCl concentration, DnaK is monomeric, and the sole effect of ATP binding to DnaK is to induce a global conformational change in DnaK, manifested as a small increase in R_g. This increase presumably also occurred upon the addition of ATP at high Tris·HCl concentration, but is masked by the much larger effect due to multimer dissociation induced by ATP (Figure 2).

The conformational change induced in DnaK by ATP binding is also supported by the observation of changes in the Kratky plot and $P(r)$ function (Figures 7 and 11). The addition of ATP results in a shift in the first peak of the $P(r)$ function to larger distance value and an increase in its d_{max} from 112 to 123 Å. From the Kratky plot, it can be seen that the major peak shifts to the smaller angle region, suggesting an increase in the size of the protein due to the addition of ATP, since the peak position at lower Q corresponds to larger R_g (Kataoka et al., 1995). A small increase in the R_s value (1−2 Å) of DnaK induced by ATP binding was observed as well by SEC−HPLC (Figure 5a). An ATP-induced conformational change was previously proposed, both theoretically and based on changes in the intrinsic fluorescence of DnaK on binding ATP (Palleros et al., 1993a) as well as the results of trypsin digestion (Liberek et al., 1991a,b).

Effects of Substrate Protein on DnaK. At high Tris·HCl concentration, and in the absence of substrate protein, the majority of DnaK is in its dimeric form, which gives an average R_g value as large as 57 Å and a d_{max} around 150 Å (Table 1 and Figure 6). The addition of substrate protein, NCA-SNase or RCMLA, results in a significant decrease in both R_g and d_{max} values. On the other hand, at low Tris·HCl concentration, addition of substrate protein results in an increase in both R_g and d_{max} values (Table 1). For both cases, the final R_g and d_{max} values both approach similar values (Table 1). In the case of high Tris·HCl, the decrease in R_g and d_{max} values is due to the dissociation of DnaK multimers induced by formation of the complex between DnaK and substrate protein. This substrate protein-induced multimer (dimer) dissociation is clearly shown by SEC−HPLC analysis (Figure 5b). For the case of low Tris·HCl, the majority of DnaK is in its monomeric form; thus, binding of substrate protein results in an increase in the size of scattering particle as reflected by the increase in R_g and d_{max} values. These change are also reflected by the changes in the $P(r)$ function (Figure 8). As can be seen from Figure 8, complex formation results in a change in the scattering particle from a dumbbell to a more globular shape. These facts, in conjunction with the measured R_s, R_g, and d_{max} values, demonstrate that the functional form of DnaK is the monomeric form (Palleros et al., 1993c).

Both the R_s (from SEC−HPLC, Figure 5) and R_g (from SAXS, Table 1) values indicate that the overall structure of the DnaK−NCA-SNase complex is slightly more compact than that of the DnaK−RCMLA complex. A difference in the $P(r)$ function between complexes of DnaK−RCMLA and DnaK−NCA-SNase is also seen in Figure 8: the DnaK−RCMLA complex also having a larger d_{max} than that for DnaK−NCA-SNase [the two substrate proteins, RCMLA and NCA-SNase, have very similar molecular weights, and both show a 1:1 molar stoichiometry with DnaK (Palleros et al., 1994b)]. Our previous work suggests that there are some differences in the overall conformation of RCMLA and NCA-SNase when bound to DnaK (Palleros et al., 1994a). The complexes of DnaK with NCA-SNase and RCMLA were formed at 37 °C, where both substrate proteins were unfolded. The SAXS and HPLC measurements were carried out at room temperature where NCA-SNase is folded and RCMLA remains unfolded. Therefore, under the experimental measurement condition, it is very likely that the unbound part of RCMLA in the complex is relatively more extended or flexible than that of NCA-SNase, resulting a larger d_{max}.

The R_g values obtained from the Guinier approximation and from the $P(r)$ function both indicate that the sizes of the DnaK−RCMLA and DnaK−NCA-SNase complexes are larger than DnaK (∼42 vs 37.5 Å); however the increase in size on forming the complex is much less than would be expected if the complex involved the substrate protein bound to the exterior of DnaK. In fact, if substrate protein binding does not perturb the overall DnaK protein shape, and the complex has a similar compactness to DnaK, then the R_g of the complex can be estimated from the relation $R_g = R_s/1.08 = 46-47$ Å. Thus, the observed R_g value is significantly smaller than the calculated value. This suggests that the substrate protein may bind in a cavity or groove of DnaK, which results in an increase in the apparent compactness of the complex, since R_g is a function of mass distribution, as explained by the simple model of Paradossl (1993).

Guanidine Hydrochloride-Induced Molten Globule State of DnaK. Recently SAXS has been used in a number of protein folding studies (Lattman, 1994) of smaller proteins, such as apomyoglobin (Kataoka et al., 1995; Eliezer et al., 1993b), cytochrome c (Kataoka, 1993), and staphylococcal nuclease (Flanagan et al., 1992). These investigations have provided significant information on native, intermediate, and unfolded states, although most of these small proteins have previously been characterized by NMR and X-ray crystallographic techniques. DnaK is a much larger protein and thus not suited for folding studies by NMR techniques, and as noted, no crystal structural information for the intact molecule is currently available. The advantage of using SAXS to investigate the folding of molecules such as DnaK is that there is no limitation on molecular size or shape, as long as the sample is homogeneous. Figure 13 shows the Kratky plots of DnaK at different Gdn·HCl concentration corresponding to the conditions in which native (N), intermediate (I), and unfolded (U) states are populated (Palleros et al., 1993b). It can be seen that at 0.6 M Gdn·HCl, the Kratky plot shows the typical features of a molten globule conformation (Kataoka et al.; 1993, Lattman, 1994). This is consistent with our previous observation by SEC−HPLC, CD, and fluorescence (Palleros et al., 1993b). The R_g values of these states (N, I, and U) are as follows: after interparticle interference correction (concentration effect), N = 37 Å, I = ∼53 Å, and U = ∼66 Å. We have previously reported the corresponding R_s values for these states from SEC−HPLC as N = 41 Å, I = 48 Å, and U = 69 Å, respectively (Palleros et al., 1993b).

ACKNOWLEDGMENT

We thank Dr. Y. Goto, D. Hamada, and Y. Hagihara of Osaka University, Japan, for assistance with the SAXS experiments, K. Reid and M. Markey for assistance in DnaK sample preparation, and Dr. D. I. Svergun for suggesting equations for the sphere model. The small-angle X-ray scattering measurements were carried out at the Photon Factory, Tsukuba, Japan.

REFERENCES

Ang, D., Liberek, K., Skowyra, D., Zylicz, M.& Georgopoulos, C. (1991) *J. Biol. Chem. 266*, 24233−24236.

Babu, Y. S., Sack, J. S., Greenhough, T. J., Bugg, C. E., Means, A. R., & Cook, W. J. (1985) *Nature (London) 315*, 37.

Beckmann, R. B., Mizzen, L. A., & Welch, W. J. (1990) *Science 248*, 850−854.

Beltran, J. R., Mascarenhas, Y. P., Craievich, A. F., & Laure, C. J. (1990) *Eur. Biophys. J. 17*, 325−329.

Blond-Elguindi, S., Fourie, A. M., Sambrook, J. F., & Gething, M.-J. H. (1993) *J. Biol. Chem. 268*, 12730−12735.

Bole, D. G., Hendershot, L. M., & Kearny, J. F. (1986) *J. Cell Biol. 102*, 1558−1566.

Burdon, R. H. (1988) *Endeavour 12*(*3*), 133−138.

Cegielska, A., & Georgopoulos, C. (1989) *J. Biol. Chem. 264*, 21122−21130.

Chappell, T. G., Konforti, B. B., Schmid, S. L., & Rothman, J. E. (1987) *J. Biol. Chem. 262*, 746−751.

Chen, L., Gavini, N., Tsuruta, H., Eliezer, D., Burgess, B., Doniach, S. Hodgson, K. O. (1994) *J. Biol. Chem. 269*, 3290−3294.

Corbett, R. J. T., & Roche, R. S. (1984) *Biochemistry 23*, 1888−1894.

Craig, E. A. (1993) *Science 260*, 1902−1904.

Dierks, T., Klappa, P., Wiech, H., & Zimmermann, R. (1993) *Philos. Trans. R. Soc. London, B 339*, 335−341.

Dorner, A. J., Bole, D. G., & Kaufman, R. J. (1987) *J. Cell Biol. 105*, 2665−2674.

Heidorn, D. B., & Trewhella, J. (1988) *Biochemistry 27*, 909−915.

Eliezer, D., Frank, P., Gills, N., Newton, W. E., Doniach, S., & Hodgson, K. O. (1993a) *J. Biol. Chem. 268*, 20953−20957.

Eliezer, D., Chiba, K., Tsuruta, H., Doniach, S., Hodgson, K. O., & Kihara, H. (1993b) *Biophys. J.* 65, 912−917.

Ellis, R. J. (1994) *Curr. Opin. Struct. Biol. 4*, 117−122.

Fasman, G. D. (1983) *Handbook of Biochemistry & Molecular Biology*, 3rd ed., Vol. I, p 149, CRC Press, Inc., Boca Raton, FL.

Feigin, L. A., Svergun, D. I. (1987) *Structure Analysis by Small-Angle X-ray and Neutron Scattering*, Plenum Press, New York.

Flaherty, K. M., DeLuca-Flaherty, C., & McKay, D. B. (1990) *Nature 346*, 623−628.

Flaherty, K. M., McKay, D. B., Kabsch, W., & Holmes, K. C. (1991) *Proc. Natl. Acad. Sci. U.S.A.* 88, 5041−5045.

Flanagan, J. M., Kataoka, M., Shortle, D., & Engelman, D. M. (1992) *Proc. Natl. Acad. Sci. U.S.A. 89*, 748−752.

Flanagan, J. M., Kataoka, M., Fujisawa, T., & Engelman, D. M. (1993) *Biochemistry 32*, 10359−10370.

Flynn, G. C., Chappell, T. G., & Rothman, J. E. (1989) *Science* 245, 385−390.

Flynn, G. C., Pohl, J., Flocco, M. T., & Rothman, J. E. (1991) *Nature 353*, 726−730.

Frydman, J., Nimmesgern, E., Ohtsuka, K., & Hartl, F. U. (1994) *Nature 370*, 111−117.

Fujisawa, T., Ueki, T., Inoko, Y., & Kataoka, M. (1987) *J. Appl. Crystallogr. 20*, 349−355.

Gast, K., Damaschun, H., Misselwitz, R., Müller-Frohne, M., Zirwer, D., & Damaschun, G. (1994) *Eur. Biophys. J. 23*, 297−305.

Gething, M.-J., & Sambrook, J. (1992) *Nature 355*, 33−45.

Gething, M. J., McCammon, K., & Sambrook, J. (1986) *Cell 46*, 939−950.

Glatter, O., & Kratky, O. (1982) *Small Angle X-ray Scattering*, Academic Press, New York.

Guinier, A. (1939) *Ann. Phys. 12*, 161−237.

Guinier, A., & Fournet, G. (1955) *Small Angle X-ray Scattering*, John-Wiley & Sons, New York.

Hartl, F. U., & Neupert, W. (1990) *Science 247*, 930−938.

Hartl, F. U., Martin, J., & Neupert, W. (1992) *Annu. Rev. Biochem. 21*, 293−322.

Hendershot, L. M., Ting, J., & Lee, A. S. (1988) *Mol. Cell. Biol. 8*, 4250−4256.

Hendrick, J. P., & Hartl, F.-U. (1993) *Annu. Rev. Biochem. 62*, 349−384.

Hynes, T. R., Kautz, R. A., Goodman, M. A., Gill, J. F., & Fox, R. O. (1989) *Nature 339*, 73−76.

Ikura, M., Kay, L. E., & Bax, A. (1990) *Biochemistry 29*, 4659−4667.

Kang, P. J., Ostermann, J., Shilling, J., Neupert, W., Craig, E. A., & Pfanner, N. (1990) *Nature 348*, 137−143.

Kataoka, M., Head, J. F., Seaton, B. A., & Engelman, D. M. (1989) *Proc. Natl. Acad. Sci. U.S.A. 86*, 6944−6948.

Kataoka, M., Head, J. F., Vorherr, T., Krebs, J., & Carafoli, E. (1991) *Biochemistry 30*, 6247−6251.

Kataoka, M., Hagihara, Y., Mihara, K., & Goto, Y. (1993) *J. Mol. Biol. 229*, 591−596.

Kataoka, M., Flanagan, J. M., Tokunaga, F., & Engelman, D. M. (1994) in *Synchrotron Radiation in the Bioscience* (Chance, B., Deisenhofer, J., Ebashi, S., Goodhead, D. T., Helliwell, J. R., Huxley, H. E., Iizuka, T., Kirz, J., Mitsui, T., Rubenstein, E., Sakabe, N., Sasaki, T., Schahl, G., Schumann, H. B., Wuthrich, K., & Zaccai, G., Eds.) pp 187−194, Clarendon Press, Oxford.

Kataoka, M., Nishii, I., Fujisawa, T., Ueki, T., Tokunaga, F., & Goto, Y. (1995) *J. Mol. Biol.* 249, 215−228.

Kaumaya, P. T. P., Berndt, K. D., Heidorn, D. B., Trewhella, J., Kezdy, F. J., & Goldberg, E. (1990) *Biochemistry 29*, 13−23.

Kim, D., Lee, Y. J., & Corry, P. M. (1992) *J. Cell. Physiol. 153*, 353−361.

Kumosinski, T. F., & Pessen, H. (1985) *Methods Enzymol. 117*, 154−182.

Lam, K. T., & Calderwood, S. K. (1992) *Biochem. Biophys. Res. Commun. 184*, 167−174.

Landry, S. J., Jordan, R., McMacken, R., & Gierasch, L. M. (1992) *Nature 355*, 455−457.

Lane, D. P., Midgley, C., & Hupp T. (1993) *Philos. Trans. R. Soc. London, B 339*, 369−373.

Langer, T., Lu, C., Echols, H., Flanagan, J., Hayer, M. K., & Hartl, F. U. (1992) *Nature 356*, 683−689.

LaRossa & Van Dyk (1991) *Mol. Microbiol. 5*, 529−534.

Lattman, E. E. (1994) *Curr. Opin. Struct. Biol. 4*, 87−92.

Lattman, E. E., Fiebig, K. M., & Dill, K. A. (1994) *Biochemistry 33*, 6158−6166.

Liberek, K., Osipuk, J., Zylicz, M., Ang, D., Skorko, J., & Georgopoulos, C. (1990) *J. Biol. Chem. 265*, 3022−3029.

Liberek, K., Skowyra, D., Zylicz, J., Johnson, C., & Georgopoulos, C. (1991a) *J. Biol. Chem. 266*, 14491−14496.

Liberek, K., Marszalek, J., Ang, D., Georgopoulos, C., & Zylicz, M. (1991b) *Proc. Natl. Acad. Sci. U.S.A. 88*, 2874−2878.

Luzzati, V., Witz, J., & Nicolaieff, A. (1961) *J. Mol. Biol. 3*, 367.

Marshall, J. M., Brown, A. J., & Ponting, C. P. (1994) *Biochemistry 33*, 3599−3606.

McCarty, J. S., & Walker, G. C. (1991) *Proc. Natl. Acad. Sci. U.S.A. 88*, 9513−9517.

McDonald, R. C., Engelman, D. M., & Steitz, T. A. (1979) *J. Biol. Chem. 254*, 2942−2943.

McKay, D. B. (1994) reported at *Cold Spring Harbor 1994 May meeting* (*The Biology of Heat Shock Proteins and Molecular Chaperones*).

Moore, P. B. (1980) *J. Appl. Crystallogr. 13*, 168−175.

Morimoto, R. I., Tissieres, A., & Georgopoulos, C., Eds. (1990) *Stress Proteins in Biology & Medicine*, Cold Spring Harbor Laboratory Press, Cold Spring Harbor, NY.

Muller, K., Kratky, O., Roschlau, P., & Hess, B. (1972) *Hoppe-Seyler's Z. Physiol. Chem. 353*, 803−809.

Neupert, W., & Pfanner, N. (1993) *Philos. Trans. R. Soc. London B 339*, 355−262.

Nozaki, Y. (1972) *Methods Enzymol. 26*, p 43.

Pace, C. N., Shirley, B. A., & Thomson, J. A. (1989) in *Protein Structure: a practical approach* (Creighton, T. E., Ed.) p. 311, IRL, Oxford.
Palleros, D. R., Welch, W. J., & Fink, A. L. (1991) *Proc. Natl. Acad. Sci. U.S.A. 88*, 5719−5723.
Palleros, D. R., Reid, K. L., McCarty, J. S., Walker, G. C., & Fink, A. L. (1992) *J. Biol. Chem. 267*, 5279−5285.
Palleros, D. R., Reid, K. L., Shi, L., Welch, W. J., & Fink, A. L. (1993a) *Nature 365*, 664−666.
Palleros, D. R., Shi, L., Reid, K. L., & Fink, A. L. (1993b) *Biochemistry 32*, 4314−4321.
Palleros, D. R., Reid, K. L., Shi, L., & Fink, A. L. (1993c) *FEBS Lett. 336*, 124−128.
Palleros, D. R., Shi, L., Reid, K. L., & Fink, A. L. (1994a) *J. Biol. Chem. 269*, 13107−13114.
Palleros, D. R., Shi, L., Reid, K. L., & Fink, A. L. (1994b) in *Protein Techniques (VI)*, pp 467−474.
Paradossl, G. (1993) *J. Chem. Educ. 70*, 440−443.
Ponting, C. P., Holland, S. K., Cederholm-Williams, S. A., Marshall, J. M., Brown, A. J., Spragson, G., & Blake, C. C. F. (1992) *Biochim. Biophys. Acta 1159*, 155−161.
Pickover, C. A., McKay, D. B., Engelman, D. M., & Steitz, T. A. (1979) *J. Biol. Chem. 254*, 11323−11329.
Ptitsyn, O. B. (1992) in *Protein Folding* (Creighton, T. E., Ed.) pp 243−300, W. H. Freeman & Company, New York.
Sadis, S., & Hightower, L. E. (1992) *Biochemistry* 31, 9406−9412.
Schmid, S. L., Braell, W. A., & Rothman, J. E. (1985) *J. Biol. Chem. 260*, 10057−10062.
Shi, L. (1994) Ph.D. Thesis, University of California, Santa Cruz.
Shi, L., Palleros, D. R., & Fink, A. L. (1994) *Biochemistry 33*, 7536−7546.
Shortle, D., & Meeker, A. K. (1989) *Biochemistry 28*, 936−944.
Svergun, D. I., Semenyuk, A. V., & Feigin, L. A. (1988) *Acta Crystallogr. A44*, 244−250.
Ungermann, C., Neupert, W., & Cyr, D. M. (1994) *Science 266*, 1250−1253.
Welch, W. J. (1993) *Philos. Trans. R. Soc. London B 339*, 327−333.
Wickner, W. T. (1994) *Science 266*, 1197−1198.

BI951984L